Available online at www.sciencedirect.com
SCIENCE DIRECT®
International Journal of Thermal Sciences 44 (2005) 944–952
International Journal of Thermal Sciences
www.elsevier.com/locate/ijts

Numerical computation of buoyant airflows confined to attic spaces under opposing hot and cold wall conditions

El Hassan Ridouane *, Antonio Campo, Matthew McGarry

Department of Mechanical Engineering, The University of Vermont, Burlington, VT 05405, USA

Received 24 November 2004; received in revised form 3 March 2005; accepted 16 March 2005

Available online 29 April 2005

Abstract

The present paper addresses laminar natural convection of air confined to an isosceles triangular cavity representative of conventional attic spaces in houses and buildings with pitched roofs and horizontal suspended ceilings. Detailed experimental data in terms of velocities, temperatures and wall heat fluxes has become available for attic spaces under summer and winter conditions some time ago. However, the comparison between the numerical-obtained temperatures and mean wall heat fluxes against the experimental-measurements is still lacking in the specialized literature. Two relevant cases of isosceles triangular cavities are considered: case 1, the base is cooled and the two inclined walls are symmetrically heated and case 2, the bottom base is heated and the two top inclined walls are symmetrically cooled. To perform the computational analysis, the finite volume method is the vehicle for the discretization of the conservation equations. The Boussinesqian fluid approximation is not invoked and all thermophysical properties are taken as temperature-dependent. Most numerical simulations have assumed the existence of a vertical plane of symmetry passing through the middle of the isosceles triangular cavity in order to deal with a manageable computational domain in the form of a right-angled triangle that is half the size of the isosceles triangular cavity. However, the computational domain adopted in this work has been taken as coincident with the physical domain. Overall, the numerical predictions of velocity, temperature and mean wall heat fluxes match reasonably well with the experimental measurements for the two cases under study here.

Keywords: Triangular cavity; Laminar flow; Heat transfer; Numerical computation; Experimental validation

1. Introduction

The study of natural convection heat transfer of fluids (gases and single-phase liquids) inside cavities of various shapes has been and continues to be an area of considerable interest for fundamental and applied research [1–3]. For instance, in a stationary cavity containing a fluid, natural convective motion is sustained even when small temperature differences are applied at the thermally active walls. This scenario represents an important subclass of confined natural convection flows occurring in several branches of engineering, geophysics, environmental sciences, etc.

Literally, there is a wealth of publications dealing with natural convection flows in two-dimensional cavities of square and rectangular cross-section with flat walls, as well as in cylindrical and spherical annular enclosures with curved walls. However, certain cavities occurring in engineering applications often have shapes differing from the conventional geometries customarily encountered in theoretical analyses and experimental programs. This is the case of a house or building attic, which fits into this category. The present paper pertains to the laminar natural convection of air inside conventional attic spaces of houses and buildings with pitched roofs and horizontal suspended ceilings during summer/winter conditions.

The most representative papers dealing with laminar natural convection in isosceles triangular cavities are cited chronologically in the following paragraphs. The flow and

* Corresponding author. Phone: (+802) 656 0978; fax: (+802) 656 1929.
E-mail address: eridouan@cem.uvm.edu (E.H. Ridouane).

1290-0729/$ – see front matter
doi:10.1016/j.ijthermalsci.2005.03.008

Nomenclature

A	aspect ratio of cavity, $= H/W$		
c_p	specific isobaric heat capacity	$J \cdot kg^{-1} \cdot K^{-1}$	
g	acceleration of gravity	$m \cdot s^{-2}$	
Gr_H	Grashof number, $= g\beta(T_H - T_C)H^3/\nu^2$		
$\bar{h}$	mean convective coefficient	$W \cdot m^{-2} \cdot K^{-1}$	
H	height of cavity	m	
L	inclined wall of cavity	m	
k	thermal conductivity	$W \cdot K^{-1} \cdot m^{-1}$	
$\overline{Nu}_H$	mean Nusselt number, $= \bar{h}H/k$		
p	pressure	Pa	
Pr	Prandtl number, $= \mu c_p/k$		
q_w	wall heat flux	$W \cdot m^{-2}$	
$\overline{q_w}$	mean wall heat flux	$W \cdot m^{-2}$	
Ra	Rayleigh number, $= Gr \times Pr$		
T	temperature	K	
u, v	velocities in the x- and y-directions	$m \cdot s^{-1}$	
W	base of cavity	m	
x, y	horizontal and vertical coordinates	m	
X	dimensionless horizontal coordinate, $= x/W$		
Y	dimensionless vertical coordinate, $= y/H$		
z	inclined coordinate	m	
Z	dimensionless inclined coordinate, $= z/L$		

Greek Letters

α	apex angle	°
β	coefficient of thermal expansion	K^{-1}
μ	dynamic viscosity	$kg \cdot m^{-1} \cdot s^{-1}$
ν	kinematic viscosity	$m^2 \cdot s^{-1}$
θ	dimensionless temperature, $= (T - T_C)/(T_H - T_C)$	
ρ	density	$kg \cdot m^{-3}$
ψ	stream function, $u = \partial\psi/\partial y$, $v = -\partial\psi/\partial x$	$m^2 \cdot s^{-1}$

Subscripts

C	cold wall
H	hot wall

temperature patterns, local wall heat fluxes and mean heat flux rates in isosceles triangular cavities with three different aspect ratios were measured experimentally by Flack [4,5]. Three cavity shapes filled with air were heated/cooled from the bottom wall and cooled/heated from the above inclined walls covering a wide range of Grashof numbers between 10^5 and 3×10^6. Akinsete and Coleman [6] conducted a finite-difference study of the natural convection flow of air contained in a right-triangular cavity (half of the isosceles triangular cavity) with a cold horizontal base and heat input through the hypotenuse and insulated vertical wall. Numerical solutions were obtained for height-base ratios $\leqslant 0.5$ in conjunction to different Grashof numbers up to a maximum Gr of 8000. Poulikakos and Bejan [7] reported a theoretical and numerical study of the fluid mechanics inside a right triangular cavity with cold upper inclined wall, warm horizontal bottom wall and insulated vertical wall. The theoretical flow and temperature fields were determined on the basis of an asymptotic analysis valid for shallow spaces with aspect ratios approaching zero. Another phase of the study focused on the temporal evolution of the velocity and temperature fields utilizing various aspect ratios of 0.2, 0.4 and 1.

Based on a stream function/vorticity formulation, Del Campo et al. [8] examined the entire isosceles triangular cavities for seven possible combinations of hot wall, cold wall and insulated wall using the finite element method. For the particular case of heating from below and cooling it from above, the computed solutions revealed the existence of symmetric velocity and temperature fields with respect to the mid plane of symmetry in a cavity with aspect ratio of one for low Grashof numbers. Salmun [9] examined a two-dimensional right triangular cavity filled with air or water with various aspect ratios and Rayleigh numbers. Solutions of the time dependent conservation equations were obtained using two different numerical techniques which while yielding different numerical values for the velocity and temperature fields, did not altered the flow structure of a single convective cell for low Ra and to multi-cellular regime for high Ra. Asan and Namli [10] conducted a numerical study of laminar natural convection in a pitched roof of triangular cross-section considering an adiabatic mid-plane wall condition in their numerical procedure. Only summertime conditions were considered over wide ranges of both the Rayleigh number and the height-based aspect ratio. Their results show that most of the heat exchange takes place near the intersection of the active walls. The finite-element-method was employed by Holtzmann et al. [11] to model the complete isosceles triangular cavity without claiming cavity symmetry. A heated horizontal base and symmetrically cooled upper tilted walls for aspect ratios of 0.2, 0.5 and 1.0 and various Grashof numbers ranging from 10^3 to 10^5 were used. These authors also conducted a flow visualization study to validate experimentally the existence of symmetry-breaking bifurcations in one cavity of fixed aspect ratio. This anomalous bifurcation phenomenon intensified with gradual increments in Gr. The major conclusion drawn in this paper was that for identical isosceles triangular cavities engaging the symmetrical and non-symmetrical assumptions, the differences in the mean Nusselt number were of the order of 5%. This indeed is the thermal quantity of interest for heat transfer calculations. It is worth adding that the majority of works cited above have assumed the existence of a vertical plane of symmetry passing through the middle of the isosceles triangular cavity in order to deal with a manageable computational domain that is half the size of the physical domain. Two years latter, assuming a symmetrical nature of the

flow within an attic space, Haese and Teubner [12] investigate the thermal effects in building attics involving ceiling fans. The problem has been solved for the winter conditions using the vorticity-stream function formulation.

Despite that experimental data for velocities, temperatures and wall heat fluxes became available for two decades for the pair realistic heating/cooling combinations in isosceles triangular cavities, not a single author has tried to compare the numerically-obtained temperatures and wall heat fluxes against the measured quantities in the elapsed years. The present work seeks to fill this gap. The aim here is to obtain numerically the detailed velocity and temperature fields of buoyant air inside isosceles triangular cavities resembling spaces bounded by two pitched roofs and a horizontal suspended ceiling. From the temperature fields, the corresponding variation of local and mean wall heat fluxes at the base and the inclined wall are estimated. To the best knowledge of the authors no information is available in the archival literature that seeks to validate the computed numerical simulations with experimental measurements of the controlling thermal quantities of local and global character.

The body of the paper is divided into three sections. The physical system and the mathematical formulation are addressed in the first section. The computational procedure and its indispensable validation are explained in the second section. The third section pertains to a discussion of the numerical velocity and temperature fields as well as the total heat transfer rates across the cavity walls. Also, one-to-one comparisons between the numerical predictions and the experimental measurements of Flack [5] are included in the last section.

2. Problem formulation

The physical system sketched in Fig. 1 consists of air contained in an isosceles triangular cavity of variable apex angle α. Two relevant cases involving prescribed wall temperatures are considered: case 1, the base is cooled and the two hypotenuses are symmetrically heated and case 2, the bottom base is heated and the two top hypotenuses are symmetrically cooled. These situations are associated with the heating or cooling of typical house or building attics during the summer and winter seasons. The gravitational acceleration acts perpendicular to the base. The dimension perpendicular to the plane of the diagram is assumed to be long enough, so that the airflows may be conceived with two-dimensional motion.

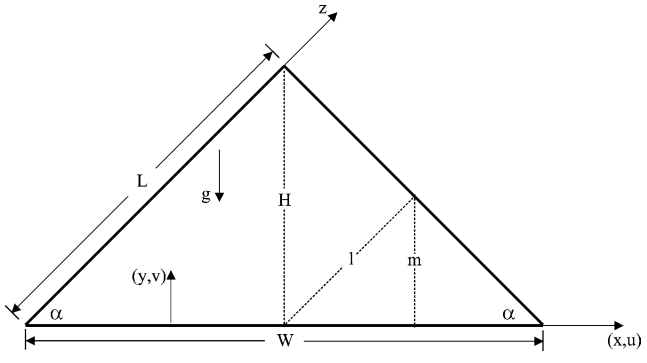

Fig. 1. Sketch of a house or building attic.

The simultaneous effect of the density, dynamic viscosity, specific heat capacity and thermal conductivity of the air changing with temperature may be important because the velocity and temperature fields can be significantly altered. Correspondingly, the standard Boussinesq approximation is not adopted and the influential thermophysical properties of air are taken as temperature-dependent. The temperature levels within the cavity are assumed to be small as to consider the effects of surface radiation upon heat transfer negligible [13]. Under the assumption of laminar regime, the two-dimensional air velocity and temperature fields obey the following system of conservation equations:

Mass:

$$\frac{\partial(\rho u)}{\partial x}+\frac{\partial(\rho v)}{\partial y}=0 \tag{1}$$

x-momentum:

$$\frac{\partial(\rho uu)}{\partial x}+\frac{\partial(\rho vu)}{\partial y}=-\frac{\partial p}{\partial x}+\frac{\partial}{\partial x}\left(\mu\frac{\partial u}{\partial x}\right)+\frac{\partial}{\partial y}\left(\mu\frac{\partial u}{\partial y}\right) \tag{2}$$

y-momentum:

$$\frac{\partial(\rho uv)}{\partial x}+\frac{\partial(\rho vv)}{\partial y}=-\frac{\partial p}{\partial y}+\frac{\partial}{\partial x}\left(\mu\frac{\partial v}{\partial x}\right)+\frac{\partial}{\partial y}\left(\mu\frac{\partial v}{\partial y}\right)+g(\rho-\rho_0) \tag{3}$$

Energy:

$$\frac{\partial(\rho uT)}{\partial x}+\frac{\partial(\rho vT)}{\partial y}=\frac{\partial}{\partial x}\left(\frac{k}{c_p}\frac{\partial T}{\partial x}\right)+\frac{\partial}{\partial y}\left(\frac{k}{c_p}\frac{\partial T}{\partial y}\right) \tag{4}$$

Ideal gas equation of state:

$$p=\rho RT \tag{5}$$

The reference density ρ_0 in the buoyancy term of Eq. (3) is evaluated at the mean temperature $T_0=(T_H+T_C)/2$. The velocity boundary conditions are based on the standard assumptions that the cavity walls are rigid and impermeable and the trapped air does not slip at the walls. Prescribed temperature boundary conditions are used in the two cases: for case 1, a cold horizontal wall and hot tilted walls and for case 2, a hot horizontal wall and cold tilted walls.

3. Numerical computations

Without any doubt, there have been considerable advances in the study of natural convection in cavities of arbitrary shape thanks to the development of potent grid generation software and efficient computational methods for

solving the proper Navier–Stokes and energy equations in non-Cartesian coordinate systems [14].

Despite that the computational domain possesses vertical symmetry, this feature is not exploited in this work, and therefore the computational domain is taken as coincident with the physical domain shown in Fig. 1.

The numerical solutions of Eqs. (1)–(5) subject to the imposed of boundary conditions determines the velocity fields $u(x, y)$, $v(x, y)$ and the temperature field $T(x, y)$ in the isosceles triangular cavities. The two controlling parameters are the apex angle and the Grashof number. The integrating of the system of partial differential equations (1)–(5) over an elementary control volume was carried out with the finite volume technique. A power law scheme is adopted for the convection-diffusion formulation. The pressure-velocity coupling is handled with the SIMPLE (semi-implicit method for pressure-linked equations) described by Patankar [15]. The Prandtl number for air is set at $Pr = 0.7$.

The local wall heat flux, q_w, can be found by applying Fourier's law at the wall evaluating the thermal conductivity of air at the mean temperature $T_0 = (T_H + T_C)/2$. This step leads to the computation of the mean wall heat flux $\overline{q_w}$ along the wall

$$\overline{q_w} = \frac{1}{L}\int_0^L q_w(z)\,\mathrm{d}z \quad \text{along the left inclined wall and}$$

$$\overline{q_w} = \frac{1}{W}\int_0^W q_w(x)\,\mathrm{d}x \quad \text{along the base wall} \tag{6}$$

The dimensionless form of the mean convective coefficient $\bar{h}$ or mean Nusselt number is

$$\overline{Nu}_H = \frac{H\bar{h}}{k} = \frac{H\overline{q_w}}{k(T_H - T_C)} \tag{7}$$

Based on several numerical experiments, the optimal computational mesh that renders a grid independent velocity and temperature fields under critical Grashof number conditions consists of 62 000 triangular elements. A non-uniform grid was deployed in the computational domain with nodes tightly clustered near the boundaries. Local convergence was assessed by monitoring the magnitude of the mean convective coefficient $\bar{h}$ along the three walls of the triangle, whereas global convergence was guaranteed by controlling the residuals of the descriptive conservation equations by setting its variations to less than 10^{-5}.

Conversely, validation of the code to predict the velocity and temperature fields in a square cavity was performed by comparing results against the benchmark solution for hot and cold vertical walls and insulated horizontal walls as found in De Vahl Davis [16]. With the computational mesh selected, the vertical velocity v, which is the essential variable in buoyancy induced flows is hardly affected by changes in the grid size. At a relatively high at $Ra_H = 10^6$ the maximum value of the dimensionless vertical velocity $V_{\max} = 221.80$ is within five percent of the benchmark results of 217.36 by De Vahl Davis [16]. Further, the overall energy balance, written in terms of the integrated heat transfer rate through the thermally active walls, must be equal. Agreements to less than 1% of the total mean Nusselt number $\overline{Nu}_H$ were found for $Ra_H = 10^6$, namely 8.75 in this work and 8.799 by De Vahl Davis.

A side comment is in order. As numerical estimations of natural convection flows in square cavities are obtained at increasingly higher Rayleigh numbers, it is natural to question the physical reality behind the solutions. By solving the steady version of the Navier–Stokes and energy equations, analysts are able to predict laminar convective flows at any Rayleigh number, in principle. Yet as the impressed wall temperature difference $(T_H - T_C)$ rises, all laminar convective flows become turbulent at sufficiently high Rayleigh numbers and many of them turn oscillatory over a range of Rayleigh numbers. The oscillatory regime usually lies somewhere in between the laminar and turbulent regimes. LeQuéré and Alziari de Roquefort [17] investigated the validity of steady solutions by way of laminar convective flows in a square cavity with top and bottom insulated walls. Using a time-dependent finite-difference code, these authors found that the onset of oscillations occurs at a Rayleigh number between 2×10^6 and 2.2×10^6. Parallel to this, in an experimental study of a square cavity with conducting horizontal walls, Briggs and Jones [18] found a transition from steady to oscillatory flow behavior at a Rayleigh number of 3×10^6. It was proclaimed in this work that the regime of periodic convective flows persisted to a Rayleigh number of at least 1.2×10^7. Based on this numeric-experimental background, we limited our numerical calculations to Rayleigh numbers $\leqslant 10^6$ for case 2. However, case 1 is more stable even at higher Rayleigh number [5] and the range of this parameter is prolonged up to 2.1×10^6.

4. Experimental validation

Three triangular isosceles cavities filled with air ($Pr = 0.7$) forming apex angles of $\alpha = 30°$, $45°$ and $60°$ were tested by Flack [5] for the two heating/cooling wall conditions cited before. The three aspect ratios chosen by this author were $A = H/W = 0.289$ for $\alpha = 30°$, 0.5 for $45°$ and 0.865 for $60°$. The wall temperatures were measured with copper constantan thermocouples and were uniform within 0.5 °C. A Wollaston prism schlieren interferometer was utilized to make the heat transfer measurements. The thermophysical properties of air were evaluated at the mean air temperature $T_0 = (T_H + T_C)/2$. Further details about the experimental set up, the measuring techniques and the data analysis are omitted for brevity but the interested reader may found them in Flack [5]. Among the three apex angles selected by Flack [5], we chose the intermediate value of $\alpha = 45°$ as representative of the set of three to run the numerical sim-

ulations under the influence of different Grashof numbers based on the cavity height H.

Case 1—Cold base and hot inclined walls

Two Grashof numbers, $Gr_H = 4.9 \times 10^5$ and 2.84×10^6, were considered by Flack [5] to the isosceles triangular configuration with an apex angle $\alpha = 45°$ to conduct the experimental measurements. Fluid motion was set up by symmetrically heating the two inclined sides while the base was maintained cold. The numerical computations were performed for several Grashof numbers, but to save journal space results have been reported for only two $Gr_H = 10^5$ and 2.84×10^6.

When examining Fig. 2(a) we observe a contour plot of the stream functions associated with $Gr_H = 10^5$ where two symmetric counter rotating vortices exist on each side of the isosceles triangle. As evident from the gradient of the stream function the velocity will be the highest near the bottom corners of the triangle, where the gradient between the stream functions is the largest. This high velocity moves the fluid from the bottom of the triangle up through the center. In contrast to the corner of the triangle, the center of the geometry contains slow moving fluid as shown by the low gradient area in the center of the triangle. When Gr_H is increased to 2.84×10^6, the qualitative shape of the counter rotating cells remains the same as reflected in Fig. 3(a). However, the magnitude of the velocity gradients in the corner increases by one order of magnitude and consequently creates higher fluid velocities. Because the top walls are heated and the bottom walls are cooled, regardless of the value of Gr_H, case 1 is always stable and the stratified temperature profiles in Figs. 2(b) and 3(b) resemble pure conduction situations.

Fig. 4(a) displays the computed temperature variation along the mid-plane of the isosceles triangular cavity for the highest Grashof number $Gr_H = 2.84 \times 10^6$ used by Flack [5]. It is observable in the figure that the air is nearly isothermal in the upper part of the cavity between the locations $Y = 0.6$ and $Y = 1$, so that in this region the heat is transferred by conduction. When compared against the experimental observations of Flack [5], the temperatures exhibit the correct trends and more important the agreement is excellent. Lines l and m in Fig. 1 identify two planes that occupy the region that lies between the mid-plane and the lower vertex. For the same large Gr_H, it is seen in Fig. 4(b) and (c) that the temperature profiles retain their shapes that are nearly identical. With respect to Fig. 4(a), it is seen that the temperature curves are pushed down and moved toward the lower right part of the plane in concordance with the conduction behavior that predominates in this region.

A key comparison between the numerical and experimental wall heat flux distribution along the hypotenuse is illustrated in Fig. 5 for $Gr_H = 2.84 \times 10^6$. Taking into consider-

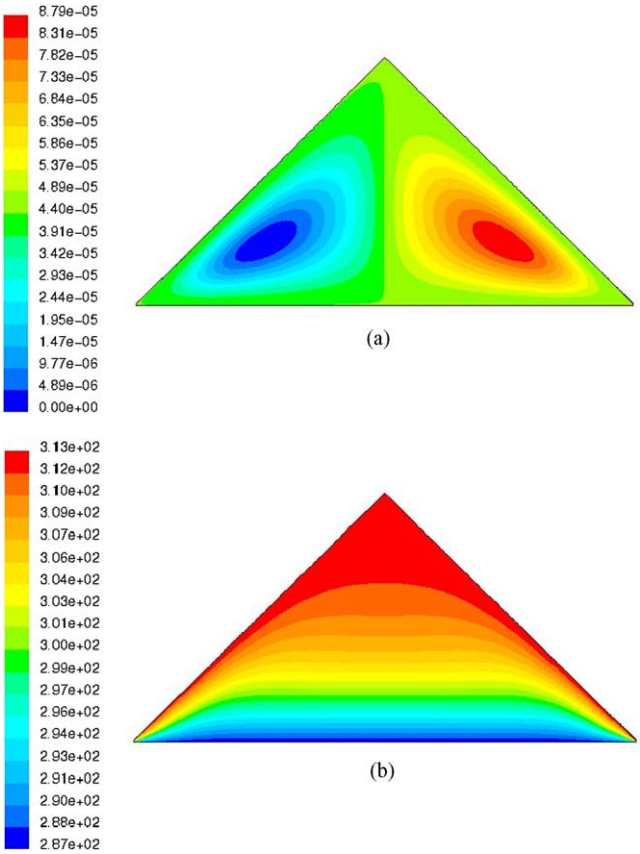

Fig. 2. Plots of stream functions and isotherms for case 1 with $Gr_H = 10^5$.

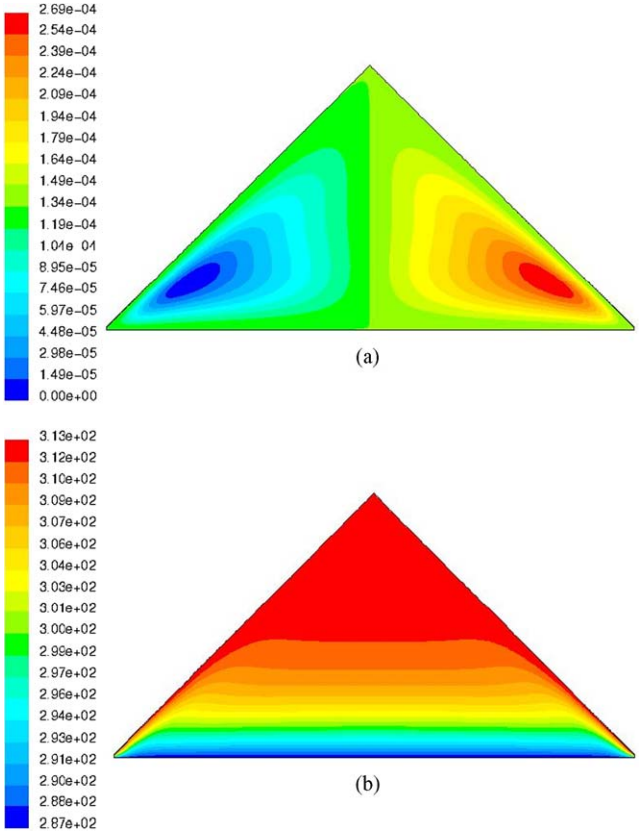

Fig. 3. Plots of stream functions and isotherms for case 1 with $Gr_H = 2.84 \times 10^6$.

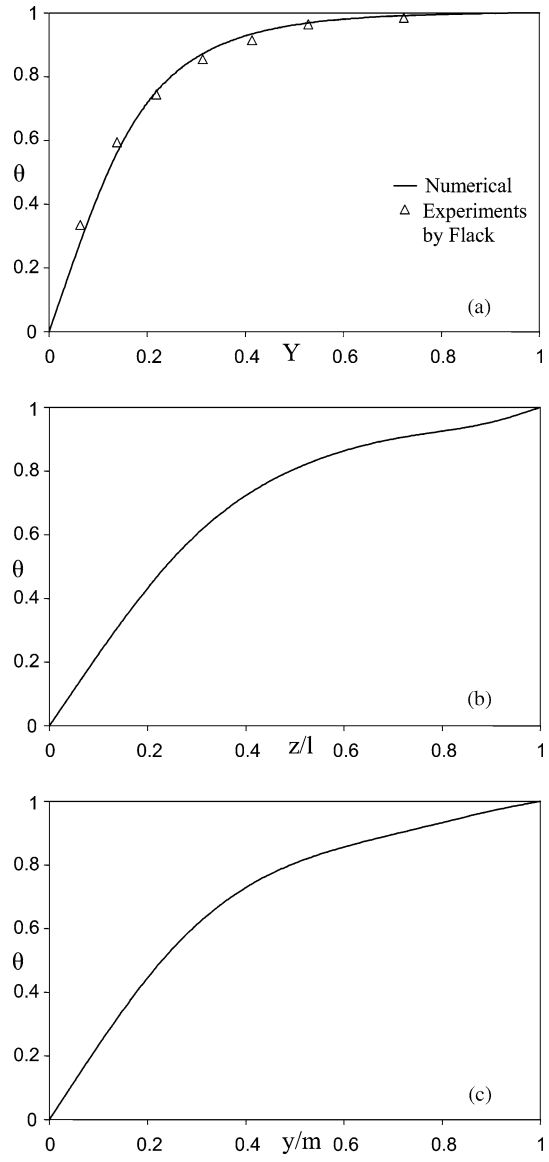

Fig. 4. Temperature variation along three different planes for case 1 with $Gr_H = 2.84 \times 10^6$.

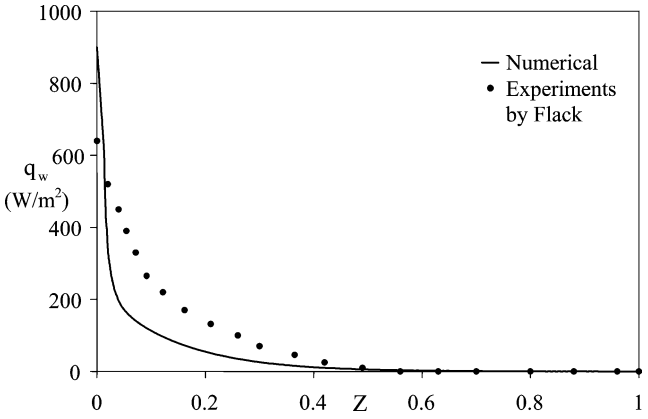

Fig. 5. Comparison between the numerical and experimental wall heat flux distributions for case 1.

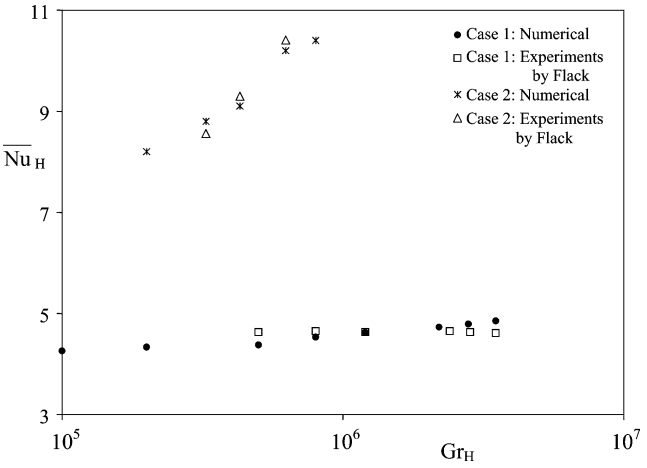

Fig. 6. Comparison between the numerical and experimental mean Nusselt numbers for cases 1 and 2.

Table 1
Conduction contribution to the heat transfer in case 1

Gr_H	10^3	10^4	10^5	3×10^5	8×10^5	2.84×10^6
Conduction contribution [%]	100	99.82	97.04	94.74	93.06	89.31

ation that the temperature discontinuity at the base/inclined wall intersection $Z = 0$ affects both the calculations and the measurements adversely, the proximity between the two exponentially decreasing wall heat flux curves is reasonable. Overall, the numerical wall heat fluxes slightly underpredict the experimental wall heat fluxes and maximum difference go up to 35%. According to Flack [5], the uncertainties of the measured wall heat fluxes were typically of the order of 8%. The high wall heat fluxes that occur near the base/inclined wall intersection are an indication that a disproportionate amount of heat is transferred across the horizontal base wall. Actually, from a qualitative standpoint, all the heat activity takes place in the first part of the hypotenuse that lies between the vertex $Z = 0$ and 0.5, whereas the second part for $Z > 0.5$ is thermally inactive.

Fig. 6 illustrates the excellent parity between the experimental $\overline{Nu}_H$ and the numerical $\overline{Nu}_H$, which stays around 4.63. The invariance of $\overline{Nu}_H$ with Gr_H indicates that the majority of the heat is transported by conduction in a relatively large Gr_H interval that spans from 2×10^5 to 2.84×10^6.

For the cavity with hot top wall, the heat transfer is dominated by conduction. A summary of the conduction contribution to the heat transfer appears in Table 1. These values are referred to the $\overline{Nu}_H$ associated to $Gr_H = 10^3$ where the heat transfer is by pure conduction. It can be noticed that the contribution by conduction gets reduced to 85% at a large $Gr_H = 2.84 \times 10^6$.

Case 2—Hot base and cold inclined walls

At small values of Gr_H below the critical $Gr_{H,C}$ there is little increase in the heat transfer over that due to conduction.

As Gr_H increases, the flow regimes include conduction, transition and boundary layer. This results in a significant increment in the mean convective coefficient $\bar{h}$. The conduction regime is characterized by a linear temperature variation in the central region of the isosceles triangular cavity. In the boundary layer regime, thin boundary layers appear along the heated wall with temperature uniformity between the lower and upper boundary layers.

Two Grashof numbers, one $Gr_H = 3.25 \times 10^5$ and the other 6.25×10^5, were assigned by Flack [5] to the cavity configuration with an apex angle $\alpha = 45°$ to conduct the experimental measurements. Based on the observations made by Flack [5] during the course of the experiments, he pointed out that the buoyant flow was initially laminar for relatively low Grashof numbers, but as the Grashof number was gradually increased the flow became turbulent. He inferred that the threshold between laminar to turbulent regimes takes place at a critical $Gr_{H,C} = 8.88 \times 10^5$.

The results are reported for two Grashof numbers $Gr_H = 2 \times 10^5$ and 6.25×10^5 ($Gr_H < Gr_{H,C}$ where the flow is steady and laminar).

In sharp contrast to Figs. 2(a) and 3(a), the symmetry between the two counter rotating vortices disappears when the prescribed temperature boundary conditions are reversed. In Fig. 7(a) for $Gr_H = 2 \times 10^5$, one cell increases in size and moves from the corner of the isosceles triangle towards the center while the second cell remains in the corner but diminishes in size. The high velocity area now exists between the two cells where the stream function gradient is high. This large velocity moves warm air from the bottom of the geometry upwards. As the fluid moves upwards the large clockwise rotating vortex in the center turns the fluid. This upward movement with turning can be seen in the temperature contours in Fig. 7(b). As the Grashof number is increased to 6.25×10^5, three rotational cells exist as evidenced in Fig. 8(a). Two of the cells are in a similar location to Fig. 7(a), but a new cell forms in the right hand corner. This new cell again moves warm fluid up from the bottom wall and helps increase the overall heat transfer from the bottom wall. In addition to the third vortex formation, the strength of the original vortices is higher for the larger Grashof number. In fact, as the Grashof number is increased from 2×10^5 to 6.25×10^5 the gradient of the stream function increases in magnitude by one order of magnitude. The direct effect of these three vortices on the temperature field can be seen in Figs. 7(b) and 8(b), where two streams of warm fluid are diverted upward from the wall.

The centerline temperature profiles are presented in Fig. 9(a) for the highest $Gr_H = 6.25 \times 10^5$ tested by Flack [5]. In this figure large temperature drops are manifested near the top and bottom of the cavity, i.e., in the segments occupied by $Y < 0.2$ and $Y > 0.8$, respectively.

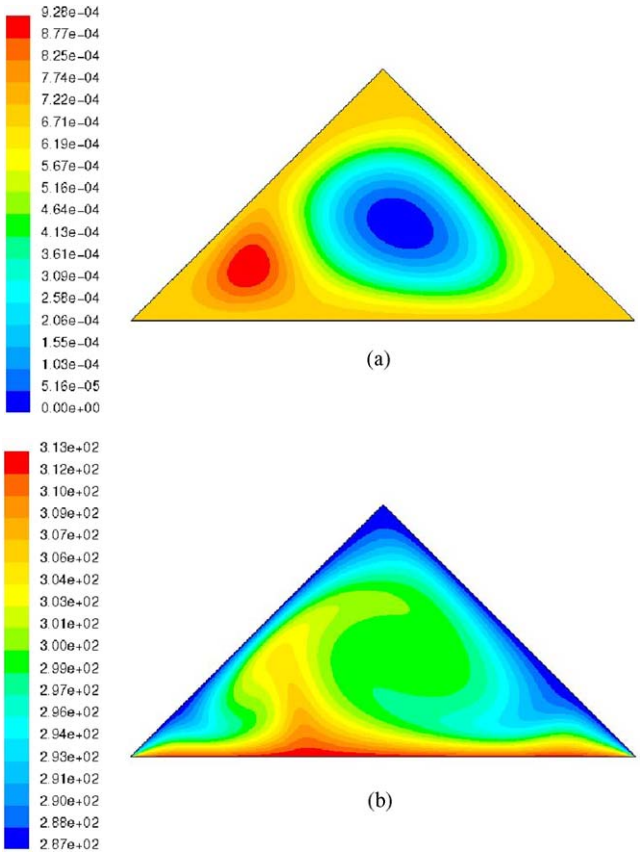

Fig. 7. Plots of stream functions and isotherms for case 2 with $Gr_H = 2 \times 10^5$.

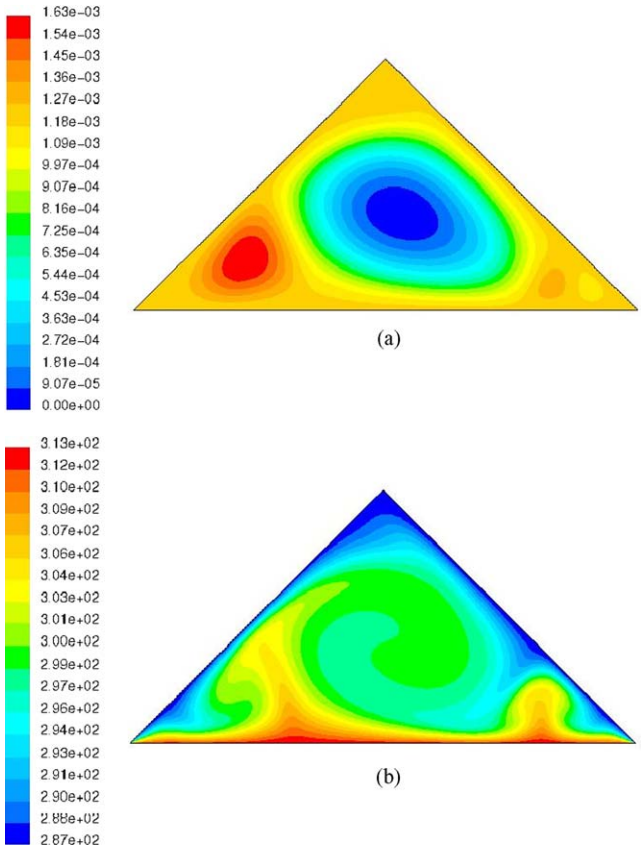

Fig. 8. Plots of stream functions and isotherms for case 2 with $Gr_H = 6.25 \times 10^5$.

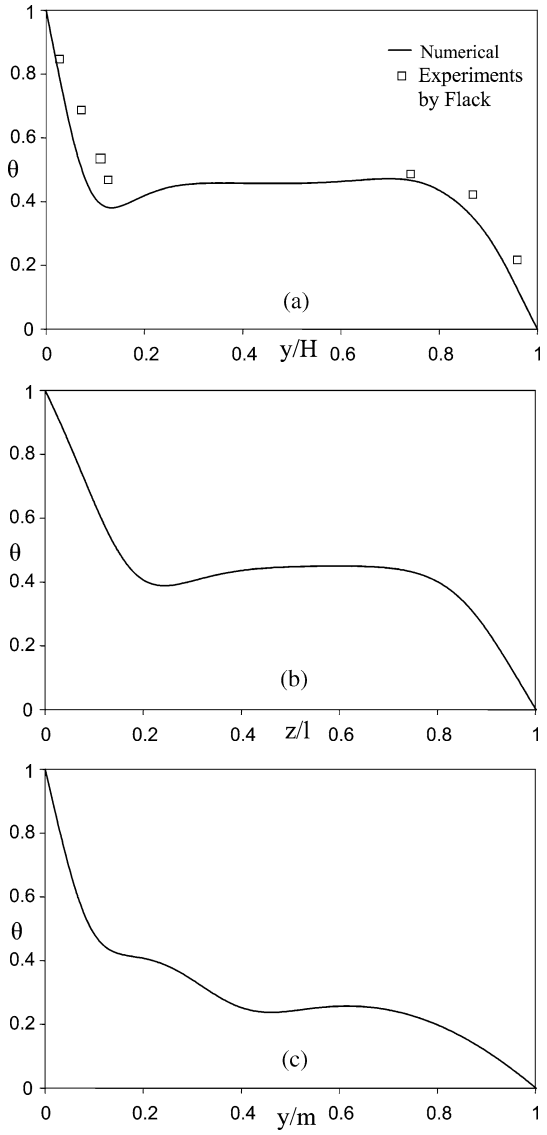

Fig. 9. Temperature variation along three different planes for case 2 with $Gr_H = 6.25 \times 10^5$.

The remaining central portion of the cavity stays isothermal around a constant temperature of $\theta = 0.5$. The agreement between the numerical and experimental temperatures is adequate. As noted before, the lines *l* and *m* in Figs. 9(b) and (c) identify two planes that occupy the region lying between the mid-plane and the apex (see Fig. 1). For the same large $Gr_H = 6.25 \times 10^5$, it is seen that the temperature profiles in Fig. 9(a) and (b) do not experience significant changes. However, the temperature curve for line m in Fig. 9(c) has been straightened in the vicinity of the abscissa.

Fig. 10 portrays the monotonic decreasing behavior of the wall heat flux q_w along the entire base. A peak and a valley is observable at a quarter distance from the base/hypotenuse intersections. Although a mismatch between the numerical and experimental curves is palpable, the path followed by the two wall heat flux curves is consistent with the physics of the problem. That is, high magnitudes of q_w close to the two

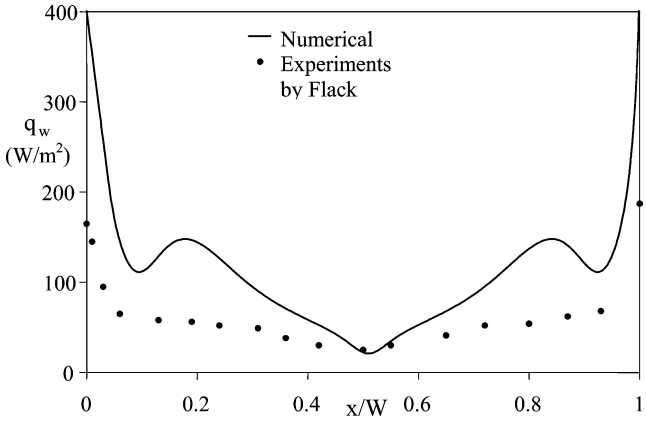

Fig. 10. Comparison between the numerical and experimental wall heat flux distributions for case 2.

ends $X = 0$ and 1, and low magnitudes of q_w near the middle part $X = 0.5$. The uncertainties of the wall heat fluxes q_w reported by Flack [5] were typically of the order of 8%.

The wall heat flux measurements q_w vs. X produced by the various Gr_H was transformed into mean wall heat fluxes $\overline{q_w}$ and thereafter into Nusselt numbers $\overline{Nu}_H$. The outcome of this operation is plotted in Fig. 6. Here, it is gratifying to see the perfect overlapping between the numerical-determined $\overline{Nu}_H$ and the experimental-observed $\overline{Nu}_H$ within the bounds of laminar air motion. In the curve-fitting sense, Flack [5] constructed three correlation equation equations, one for each apex angle $\alpha = 30°$, 45° and 60°. This individualized approach leaves a lot to be desired. In contrast, we looked into a big picture embracing the three apex angles $\alpha = 30°$, 45° and 60°. The comprehensive correlation equation turns out to be

$$\overline{Nu}_H = 0.286A^{-0.286}Gr_H^{1/4} \tag{8}$$

which portrays a correlation coefficient $R^2 \approx 0.975$. It is recognizable that the structure of this correlation equation is consistent with those correlations inherent to natural convection in closed spaces as reported in Yang [1], Raithby and Hollands [2] and Jaluria [3]. At this point, it is worth commenting also about the exponents showing up in Eq. (8). First, the universal exponent 1/4 in Gr_H is prototypical of laminar regimes. Secondly, the negative exponent affecting the aspect ratio A is essentially a trademark for laminar natural convection in vertical rectangular and square cavities. The existence of a negative-sloped linear relationship between the $\log(\overline{Nu}_H/Gr_H^{1/4})$ and the $\log A$ for the three apex angles reconfirms the adherence to the physics of the problem.

As before, it may be of interest to quantify the contribution of conduction to the total heat transfer across the cavity. The computed results are summarized in Table 2. The heat transfer domination by conduction is not as pronounced as in the case 1 when the cavity was heated from the top. For instance, at a common value of $Gr_H = 8 \times 10^5$, the contribution of conduction comes down to 61%, whereas for the other case was 93%.

Table 2
Conduction contribution to the heat transfer in case 2

Gr_H	10^3	10^4	10^5	3.25×10^5	6.25×10^5	8×10^5
Conduction contribution [%]	100	97.56	80.93	71.44	63.88	61.42

5. Concluding remarks

When the top walls of an isosceles triangular cavity are symmetrically heated and the bottom wall is cooled as in case 1, the velocities and temperatures are always stable regardless of the value of Gr_H. Under these circumstances, the stratified temperature profiles resemble pure heat conduction and the experimental and the numerical $\overline{Nu}_H$ stay around 4.63. This is indicative that the heat is transported by conduction in a relatively large Gr_H interval up to 2.84×10^6. For case 2, an isosceles triangular cavity with symmetrically cooled top walls and heated bottom wall, the flow structure is non-symmetrical for the range of Gr_H considered. Two vortices of different sizes are present; the main vortex and secondary vortex in the left corner. Another secondary vortex appears in the right corner when the Grashof number was gradually increased. In terms of heat transfer, as Gr_H increases, the flow regimes include conduction, transition and boundary layer resulting in a significant increment in the mean convective coefficient $\bar{h}$. Starting at the critical hot/cold wall intersection, the local wall heat flux q_w exhibits a monotonic decreasing path along the entire base W. Good agreement is obtained between the numerical predictions and the experimental measurements of $\overline{Nu}_H$ (a global quantity). This lends credibility to the numerical simulation of laminar buoyant air inside a wide variety of attic spaces.

References

[1] K.T. Yang, Natural convection in enclosures, in: S. Kakac (Ed.), Handbook of Single-Phase Heat Transfer, Wiley, New York, 1987, Chapter 13.

[2] G.D. Raithby, K.G.T. Hollands, Natural convection, in: W.M. Rohsenow (Ed.), Handbook of Heat Transfer, third. ed., McGraw-Hill, New York, 1998, Chapter 4.

[3] Y. Jaluria, Natural convection, in: A. Bejan, A.D. Kraus (Eds.), Heat Transfer Handbook, Wiley, New York, 2003, Chapter 7.

[4] R.D. Flack, Velocity measurements in two natural convection air flows using a laser velocimeter, J. Heat Transfer 101 (1979) 256–260.

[5] R.D. Flack, The experimental measurement of natural convection heat transfer in triangular enclosures heated or cooled from below, J. Heat Transfer 102 (1980) 770–772.

[6] V.A. Akinsete, T.A. Coleman, Heat transfer by steady laminar free convection in triangular enclosures, Internat. J. Heat Mass Transfer 25 (1982) 991–998.

[7] D. Poulikakos, A. Bejan, The fluid mechanics of an attic space, J. Fluid Mech. 131 (1983) 251–269.

[8] E.M. Del Campo, M. Sen, E. Ramos, Analysis of laminar natural convection in a triangular enclosure, Numer. Heat Transfer 13 (1988) 353–372.

[9] H. Salmun, Convection patterns in a triangular domain, Internat. J. Heat Mass Transfer 38 (1995) 351–362.

[10] H. Asan, L. Namli, Laminar natural convection in a pitched roof of triangular cross section: summer day boundary condition, Energy Buildings 33 (2000) 69–73.

[11] G.A. Holtzmann, R.W. Hill, K.S. Ball, Laminar natural convection in isosceles triangular enclosures heated from below and symmetrically cooled from above, ASME J. Heat Transfer 122 (2000) 485–491.

[12] P.M. Haese, M.D. Teubner, Heat exchange in an attic space, Internat. J. Heat Mass Transfer 45 (2002) 4925–4936.

[13] B. Gebhart, Y. Jaluria, R.L. Mahajan, B. Sammakia, Buoyancy-Induced Flows and Transport, Hemisphere, New York, 1988.

[14] J.C. Tannehill, D.A. Anderson, R.H. Pletcher, Computational Fluid Mechanics and Heat Transfer, Taylor and Francis, Washington, DC, 1997.

[15] S.V. Patankar, Numerical Heat Transfer and Fluid Flow, Hemisphere, Washington, DC, 1980.

[16] G. De Vahl Davis, Natural convection of air in a square cavity: A benchmark numerical solution, Internat. J. Numer. Meth. Fluids 11 (1983) 249–264.

[17] P. LeQuéré, T. Alziari de Roquefort, Transition to unsteady natural convection of air in vertical differentially heated cavities: Influence of thermal boundary conditions on the horizontal walls, in: Proc. 8th. Int. Heat Transfer Conference, San Francisco, CA, 1986.

[18] D.G. Briggs, D.N. Jones, Two-dimensional periodic natural convection in an enclosure of aspect ratio one, J. Heat Transfer 107 (1985) 850–854.